

# STRONG LENSING MODELING IN GALAXY CLUSTERS AS A PROMISING METHOD TO TEST COSMOGRAPHY I. PARAMETRIC DARK ENERGY MODELS

JUAN MAGAÑA<sup>1</sup>

Instituto de Física y Astronomía, Facultad de Ciencias  
Universidad de Valparaíso, Avda. Gran Bretaña 1111,  
Valparaíso, Chile.

ANA ACEBRÓN

Aix Marseille Univ, CNRS, LAM, Laboratoire d'Astrophysique de Marseille, Marseille, France

VERÓNICA MOTTA

Instituto de Física y Astronomía, Facultad de Ciencias  
Universidad de Valparaíso, Avda. Gran Bretaña 1111,  
Valparaíso, Chile.

TOMÁS VERDUGO

Instituto de Astronomía, Universidad Nacional Autónoma de México, Apartado postal 106, C.P. 22800, Ensenada, B.C., México

ERIC JULLO

Aix Marseille Univ, CNRS, LAM, Laboratoire d'Astrophysique de Marseille, Marseille, France

MARCEAU LIMOUSIN

Aix Marseille Univ, CNRS, LAM, Laboratoire d'Astrophysique de Marseille, Marseille, France

<sup>1</sup>juan.magana@uv.cl

## ABSTRACT

In this paper we probe five cosmological models for which the dark energy equation of state parameter,  $w(z)$ , is parameterized as a function of redshift using strong lensing data in the galaxy cluster Abell 1689. We constrain the parameters of the  $w(z)$  functions by reconstructing the lens model under each one of these cosmologies with strong lensing measurements from two galaxy clusters: *Abell 1689* and a mock cluster, *Ares*, from the Hubble Frontier Fields Comparison Challenge, to validate our methodology. To quantify how the cosmological constraints are biased due to systematic effects in the strong lensing modeling, we carry out three runs considering the following uncertainties for the multiple images positions:  $0.25''$ ,  $0.5''$ , and  $1.0''$ . With *Ares*, we find that larger errors decrease the systematic bias on the estimated cosmological parameters. With real data, our strong-lensing constraints on  $w(z)$  are consistent those derived from other cosmological probes. We confirm that strong lensing cosmography with galaxy clusters is a promising method to constrain  $w(z)$  parameterizations. A better understanding of galaxy clusters and their environment is however needed to improve the SL modeling and hence to estimate stringent cosmological parameters in alternatives cosmologies.

*Keywords:* dark energy, strong lensing, cosmological parameters, galaxy clusters

## 1. INTRODUCTION

Current cosmological observations provide strong evidence that the expansion of the Universe is accelerating (Riess et al. 1998; Perlmutter et al. 1999; Planck Collaboration et al. 2016b). The source of this cosmic acceleration is a big puzzle in modern cosmology and two hypothesis have been proposed to explain it: either to postulate the existence of a dark energy component or to modify the gravity laws (Joyce et al. 2016). Among the first kind of models, the cosmological constant, which is commonly associated to the quantum vacuum energy, has been established as the preferred candidate to the nature of dark energy by several cosmological measurements (e.g. Planck Collaboration et al. 2016a). By definition, the equation of state (EoS, hereafter) parameter of the cosmological constant is  $w = -1$ . Nonetheless, when a general constant equation of state is considered, the data constrain  $w = -1.019_{-0.080}^{+0.075}$  (Planck Collaboration et al. 2016b, see also Neveu et al. 2017), which is consistent with the cosmological constant. In spite of this consistency, the theoretical expected value of the vacuum energy differs in many orders of magnitude from the observed one. In addition, the coincidence problem, i.e. the similitude seen at the current time between the dark matter energy density and that of DE, remains unsolved (Zeldovich 1968; Weinberg 1989). Several dark energy (DE, hereafter) models, as for instance, dynamical dark energy or interacting dark energy (Copeland et al. 2006; Li et al. 2011), are also in agreement with the data and they can satisfactorily describe the late-time acceleration of the Universe in a similar way as the cosmological constant does (Ferreira et al. 2017; Salvatelli et al. 2014; Zhao et al. 2017). Therefore, to distinguish which cosmological model is the more suitable to the nature of dark energy, we need to put tight constraints on their parameters. A standard way to estimate these parameters is to perform a Bayesian analysis using classic cosmological probes, i.e. to fit the distance modulus of type Ia distant supernovae (SNIa), Hubble parameter measurements, baryon acoustic oscillation (BAO) signal, and the acoustic peaks of the cosmic microwave background (CMB) radiation (Davis 2014; Mortonson et al. 2014). Although these tests are widely used to constrain cosmological models, they could yield to biased estimations because either the data or the test fitting formulas are derived assuming an underlying standard cosmology  $\Lambda$ CDM (i.e. the cosmological constant as dark energy plus cold dark matter). Thus, it is essential to construct methods to estimate the parameters of alternative cosmologies without assuming any fiducial cosmology. One novel technique is to use strong lensing measurements in galaxy clusters.

Strong gravitational lensing (SL, hereafter) offers a unique and independent opportunity to constrain dark energy features without prior assumptions on the fiducial cosmology. Link & Pierce (1998) introduced a new approach by leveraging the cosmological sensitivity of the angular size-redshift relation when multiples imaged systems (over a broad range of redshift) are produced by strong lensing clusters. This technique was later on extended to more complex simulated clusters by Golse et al. (2002) and to real clusters such as Abell 2218 (see Soucail et al. 2004), showing that SL cosmography is a promising geometrical cosmological test. Jullo et al. (2010) used an improved technique which simultaneously reconstructed the mass distribution of Abell 1689 (A1689, hereafter), adopting a parametric lens modeling, and constrained the parameters of a  $w$ CDM cosmology. For the first time, the authors obtained competitive constraints on the equation of state parameter and found that, by combining their results with other probes, they improved the DE EoS estimation by  $\sim 30\%$ . Following the same method, Caminha et al. (2016) recently used the SL measurements in Abell S1063 with the pre-*Frontier Fields* data to constrain cosmological parameters for three different  $\Lambda$ CDM models. They pointed out the importance of estimating the parameters using multiply lensed sources with a wide range of redshifts. The authors also showed that the lack of spectroscopic measurements or the use of inaccurate photometric redshifts leads to a biased estimation of the cosmological parameters. Magaña et al. (2015) exploited this technique too, but using alternative cosmologies. They used A1689 strong lensing measurements to constrain four dark energy models: Chevallier-Polarski-Linder (CPL), Interacting Dark Energy (IDE), Ricci Holographic Dark Energy (RHDE), and Modified Polytropic Cardassian (MPC). They found that the SL method provides CPL constraints in good agreement with those obtained with the SNe Ia, BAO and CMB data. In addition, the IDE and RHDE constraints derived from SL are similar to those estimated with other tests. Nevertheless, the IDE constraints are consistent with the complementary bounds only if an increase in the image-position error (five times the one previously used by Jullo et al. 2010) is considered in the lens modeling. They confirmed that, to avoid misleading DE bounds, it is important to consider larger positional uncertainties for the multiple images; which could be associated with systematic errors.

Indeed, SL has various known sources of systematic errors. D’Aloisio & Natarajan (2011), using simulations of cluster lenses, showed that the observational errors (for space-based images) are an order of magnitude smaller than the modeling errors. Furthermore, line-of-sight (LOS) structures can introduce a systematic error in the strong lensing

modeling (e.g. Bayliss et al. 2014; Giocoli et al. 2016; Host 2012; Jaroszynski & Kostrzewa-Rutkowska 2014; McCully et al. 2014) of up to  $\sim 1.4''$  on the position of multiple images (Zitrin et al. 2015). Even distant massive structures in the lens plane have a significant impact on the position of multiple images (Tu et al. 2008; Limousin et al. 2010). Harvey et al. (2016), by analyzing the *Frontier Field* cluster MACSJ0416 ( $z = 0.397$ ), estimated an error of  $\sim 0.5''$  on the position of the multiple images when assuming that light traces mass in the SL modeling. However, few studies have investigated their impact on the retrieval of cosmological parameters (McCully et al. 2017; Acebron et al. 2017).

In this paper, we are interested in quantifying the uncertainties in the estimation of cosmological parameters induced by different positional errors of the multiple images. To this end, we analyze the strong lensing effect in the galaxy cluster A1689, as well as in a mock galaxy cluster at  $z = 0.5$  generated in a flat  $\Lambda$ CDM cosmology. Because in the CLP case it is possible to obtain tight constraints on its parameters (see Magaña et al. 2015) using the SL methodology proposed by Jullo et al. (2010), in this work we consider popular CPL-like models in which the EoS of dark energy is parametrized as function of redshift.

The paper is organized as follows: in the next section, §2, we introduce the cosmological framework and the parametric dark energy models. In section §3 we describe the SL data and methodology used to constrain the cosmological parameters of the DE models. In section §4 we present and discuss the results. Finally, we provide our conclusions in section §5.

## 2. COSMOLOGICAL FRAMEWORK AND PARAMETRIC DARK ENERGY MODELS

For a homogeneous, isotropic, and flat Friedmann-Lemaître-Robertson-Walker (FLRW) cosmology, the expansion rate of the Universe is governed by the Friedmann equation:

$$H^2(z) \equiv \frac{8\pi G}{3} \sum_i \rho_i(z), \quad (1)$$

where  $H \equiv \dot{a}/a$  is the Hubble parameter,  $a$  is the scale factor of the Universe, and  $\rho_i$  denotes the energy density for each component in the Universe<sup>1</sup>. We consider cold dark matter ( $m$ ) and radiation ( $r$ ) components whose dynamics are described by a perfect fluid with EoS  $w_m = 0$  and  $w_r = 1/3$ , respectively. In addition, we also consider a dynamical dark energy ( $de$ ) whose EoS is parameterized by a  $w(z)$  function. In terms of the present values<sup>2</sup> of the density parameters,  $\Omega_i \equiv 8\pi G\rho_i/3H(z)^2$ , for each component, the Eq. 1 reads as:

$$E^2(z) = \Omega_m(1+z)^3 + \Omega_r(1+z)^4 + \Omega_{de}f_{de}(z), \quad (2)$$

where  $E(z) = H(z)/H_0$  is the dimensionless Hubble parameter,  $\Omega_r = 2.469 \times 10^{-5}h^{-2}(1 + 0.2271N_{eff})$ , with  $h = H_0/100\text{kms}^{-1}\text{Mpc}^{-1}$ ,  $N_{eff} = 3.04$  is the standard number of relativistic species (Komatsu et al. 2011), and  $\Omega_{de}$  can be expressed as  $\Omega_{de} = 1 - \Omega_m - \Omega_r$ . The function  $f_{de}(z)$  is defined as:

$$f_{de}(z) \equiv \frac{\rho_{de}(z)}{\rho_{de}(0)} = \exp\left(3 \int_0^z \frac{1+w(z)}{1+z} dz\right). \quad (3)$$

Notice that, by introducing a  $w(z)$  functional form in the integral of the Eq. (3), we can obtain an analytical expression for  $f_{de}(z)$ , and hence for  $E(z)$ .

Besides, to test whether the constraints for each parametric DE model result in a late cosmic acceleration, we examine the deceleration parameter  $q(z)$  defined as:

$$q(z) = -\frac{\ddot{a}(z)a(z)}{\dot{a}^2(z)}. \quad (4)$$

Using Eq. (2), we obtain:

$$q(z) = \frac{(1+z)}{E(z)} \frac{dE(z)}{dz} - 1, \quad (5)$$

which expresses the deceleration parameter in terms of the dimensionless Hubble parameter.

<sup>1</sup> dot stands for the derivative with respect to the cosmic time

<sup>2</sup> Quantities evaluated at  $z = 0$

### 2.1. Parametric dark energy models

One alternative to the cosmological constant is to consider a dark energy component which admits a time-dependent EoS. An effective and simple way to study dynamical dark energy models is to assume a phenomenological parameterization of the EoS (Lazkoz et al. 2005; Pantazis et al. 2016). Commonly, this EoS is biparametric and it depends on the scale factor of redshift. The most popular ansatz, denoted Chevallier-Polarski-Linder parameterization, (introduced and revisited by Chevallier & Polarski 2001; Linder 2003, respectively) is  $w(z) = w_0 + w_1 z / (1 + z)$ , where  $w_0$  is the present value of the equation of state and  $w_1 = dw(z)/dz|_{z=0}$ . In this paper we study five CPL-like EoS parameterizations (see Magaña et al. 2014; Wang et al. 2016, for details), in the following, we briefly introduce the functional form of these parameterizations.

- Jassal-Bagla-Padmanabhan (JBP).- Jassal et al. (2005b,a) proposed that the dark energy EoS is parameterized by the function

$$w(z) = w_0 + w_1 \frac{z}{(1+z)^2}, \quad (6)$$

which allows rapid variations at low  $z$ . The DE has the same EoS at the present epoch and at high redshift, i.e.,  $w(\infty) = w_0$ . By substituting the Eq. (6) in Eq. (3) we obtain:

$$f_{de}(z) = (1+z)^{3(1+w_0)} \exp \left[ \frac{3}{2} \frac{w_1 z^2}{(1+z)^2} \right]. \quad (7)$$

- Barbosa-Alcaniz (BA).- Barboza & Alcaniz (2008) considered a parametric EoS for the dark energy component given by:

$$w(z) = w_0 + w_1 \frac{z(1+z)}{1+z^2}. \quad (8)$$

This ansatz behaves linearly at low redshifts as  $w_0 + w_1 z$ , and  $w \rightarrow w_0 + w_1 z$  when  $z \rightarrow \infty$ . In addition,  $w(z)$  is well-behaved in all epochs of the Universe, for instance, the DE dynamics in the future, at  $z = -1$ , can be investigated without dealing with a divergence. Solving the integral in Eq. (3) and using Eq. (8) results in:

$$f_{de}(z) = (1+z)^{3(1+w_0)} (1+z^2)^{\frac{3}{2}w_1}. \quad (9)$$

- Feng-Shen-Li-Li (FSLLI, Feng et al. 2012) suggested two dark energy EoS parameterizations given by:

$$w(z) = w_0 + w_1 \frac{z}{1+z^2}, \quad \text{FSLLI} \quad (10)$$

$$w(z) = w_0 + w_1 \frac{z^2}{1+z^2} \quad \text{FSLLII}. \quad (11)$$

Both functions have the advantage of being divergence-free throughout the entire cosmic evolution, even at  $z = -1$ . At low redshifts,  $w(z)$  behaves as  $w_0 + w_1 z$  and  $w_0 + w_1 z^2$  for FSLLI and FSLLII respectively. In addition, when  $z \rightarrow \infty$ , the EoS has the same value,  $w_0$ , as the present epoch for FSLLI and  $w_0 + w_1$  for FSLLII. Using Eqs. (10)-(11) to solve Eq. (3) leads to:

$$f_{de\pm}(z) = (1+z)^{3(1+w_0)} \exp \left[ \pm \frac{3w_1}{2} \arctan(z) \right] (1+z^2)^{\frac{3}{4}w_1} (1+z)^{\mp \frac{3}{2}w_1}, \quad (12)$$

where  $f_+$  and  $f_-$  correspond to FSLLI and FSLLII respectively.

- Sendra-Lazkoz (SeLa, Sendra & Lazkoz 2012) improved the CPL parameterization, whose  $w_0 - w_1$  parameters are highly correlated and  $w_1$  is poorly constrained by the observational data, introducing new polynomial parameterizations. They are constructed to reduce the parameter correlation, so they can be better constrained by the observations at low redshifts. One of these parameterizations is given by:

$$w(z) = -1 + c_1 \left( \frac{1+2z}{1+z} \right) + c_2 \left( \frac{1+2z}{1+z} \right)^2, \quad (13)$$

where the constants are defined as  $c_1 = (16w_0 - 9w_{0.5} + 7)/4$ , and  $c_2 = -3w_0 + (9w_{0.5} - 3)/4$ , and  $w_{0.5}$  is the value of the EoS at  $z = 0.5$ . This  $w(z)$  function is well-behaved at higher redshifts as  $(-1 - 8w_0 + 9w_{0.5})/2$ . By the substitution of Eq. (13) into Eq. (3), we obtain:

$$f_{de}(z) = (1+z)^{\frac{3}{2}(1-8w_0+9w_{0.5})} \exp \left[ \frac{3z \{w_0(52z+40) - 9w_{0.5}(5z+4) + 7z+4\}}{8(1+z)^2} \right]. \quad (14)$$

By replacing the  $f_{de}(z)$  functions in Eq. (1), we obtain an analytical  $E(z)$  function for each parametric  $w(z)$ , which will be used in the following sections to estimate the EoS parameters. Our main purpose is to examine the quality of the  $w(z)$  constraints extracted from the SL modeling when different image-position errors are considered.

### 3. METHODOLOGY

#### 3.1. Strong lensing as a cosmological probe

The gravitational lensing effect is produced when the light-beam of a background source is deflected by a gravitational lens, i.e. a mass distribution between the source and the observer. We refer to the strong lensing regime when several rings, arcs or multiples images are observed as a result of the distortion and deflection of the light from a source by a lens. These strong lensing observables offer a powerful and useful tool to not only infer the total matter distribution in astrophysical systems (Jauzac et al. 2014; Monna et al. 2017), but also to provide insights on the total content of the Universe, dark matter and dark energy properties (Golse et al. 2002; Soucail et al. 2004; Jullo et al. 2010; Caminha et al. 2016; Magaña et al. 2015). Here, we use strong lensing measurements in galaxy clusters to constrain the equation of state of parametric dark energy models.

Since the strong lensing features depend on the dynamics of the Universe via the angular diameter distance between the source, lens and observer, it can be used as a geometric cosmological probe. For any underlying cosmology, the angular diameter distance ratios for two images from different sources defines the 'family ratio' (see Jullo et al. 2010, for a detailed discussion):

$$\Xi(z_1, z_{s1}, z_{s2}, \Theta) = \frac{D(z_1, z_{s1}) D(0, z_{s2})}{D(0, z_{s1}) D(z_1, z_{s2})}, \quad (15)$$

where  $\Theta$  is the vector of cosmological parameters to be fitted,  $z_1$  is the lens redshift,  $z_{s1}$  and  $z_{s2}$  are the two source redshifts, and  $D(z_i, z_f)$  is the angular diameter distance calculated as:

$$D(z_i, z_f) = \frac{r(z_i, z_f)}{(1+z_f)}, \quad (16)$$

where  $r(z_i, z_f)$ , the comoving distance of a source at redshift  $z_f$  measured by an observer at redshift  $z_i$ , is given by

$$r(z_i, z_f) = \frac{c}{H_0} \int_{z_i}^{z_f} \frac{dz'}{E(z')}. \quad (17)$$

Notice that the underlying cosmology in the lens modeling is selected by introducing the  $E(z)$  function in the Eq. (17). For the parametric DE models, these functions are analytical and  $\Theta = \{\Omega_m, w_0, w_1\}$  ( $w_{0.5}$  for the SeLa parameterization) is the free parameter vector.

#### 3.2. Lensing modeling

To constrain the parameters of the DE models presented in 2.1, we use the SL measurements in two galaxy clusters: a real one, *Abell 1689*, and a simulated one, *Ares* from the Frontier Fields Comparison Challenge (Meneghetti et al. 2016).

We performed the SL modeling using the public software LENSTOOL<sup>3</sup> (Kneib et al. 1996; Jullo et al. 2007) in which the DE cosmological models described in 2.1 were implemented. LENSTOOL is a ray-tracing code with a Bayesian Markov Chain Monte-Carlo sampler which optimizes the model parameters using the positions of the multiply imaged systems. The matter distribution in clusters is modeled in a parametric way and the optimization is performed in the image plane for *Abell 1689* as it is more precise (this is different from the analysis by Jullo et al. 2010; Magaña et al.

<sup>3</sup> <https://projets.lam.fr/projects/lenstool>

2015, where the optimization was performed in the source plane). For *Ares*, the optimization was realized in the source plane as it is a more complex cluster (more images and cluster members) and this procedure is more computationally efficient. We checked that results in the image plane were similar for a subset of calculations.

For both *Abell 1689* and *Ares*, each potential (either large or galaxy-scale) is parametrized with the Pseudo Isothermal Elliptical Mass Distribution profile (hereafter PIEMD, [Kassiola & Kovner 1993](#); [Elíasdóttir et al. 2007](#)). The density distribution of this profile is given by:

$$\rho(r) = \frac{\rho_0}{\left(1 + \frac{r^2}{r_{core}^2}\right)\left(1 + \frac{r^2}{r_{cut}^2}\right)}, \quad (18)$$

with a central density  $\rho_0$ , a core radius  $r_{core}$  and a truncation radius  $r_{cut}$ . This profile is characterized by two changes in the density slope: it behaves as an isothermal profile within the transition region but the density falls as  $\rho \propto r^{-4}$  at large radii. In LENSTOOL, it has the following free parameters: the coordinates  $x, y$ ; the ellipticity,  $e$ ; angle position,  $\theta$ ; core and cut radii,  $r_{core}$  and  $r_{cut}$  and a velocity dispersion,  $\sigma$ . Both clusters were modeled in the same way regardless of the considered DE cosmological model.

*Abell 1689*.- a massive cluster at redshift  $z = 0.18$ , is one of the most studied strong lenses (see e.g., [Limousin et al. 2007, 2013](#); [Umetsu et al. 2015](#); [Diego et al. 2015](#), and references therein). The first SL modeling was performed by [Miralda-Escude & Babul \(1995\)](#) which already required a bi-modal mass distribution for the cluster. It is one of the most X-ray luminous clusters and has a large Einstein radii,  $\sim 45''$ . A1689 is still the target of recent observations, using MUSE data [Bina et al. \(2016\)](#) confirmed or spectroscopically identified new multiples images as well as cluster members.

We refer the reader to [Jullo et al. \(2010\)](#) for a detailed discussion of the modeling of A1689, where a SL parametric model was used to constrain the DE EoS. As we follow-up their approach, we give here a quick overview. *Abell 1689* was modeled using the SL features in the deep HST observations and extensive ground-based spectroscopic follow-up. The mass distribution was represented as bi-modal, with one central and dominant large-scale potential harboring a brightest central cluster galaxy (BCG) in its centre. The second large-scale potential was situated in the north-east. [Jullo et al. \(2010\)](#) used 58 cluster galaxies (with  $m_K < 18.11$ ) in the modeling and followed the standard scaling relations. The authors included a catalog of 28 images from 12 families, all with measured spectroscopic redshifts, spanning a range of  $1.15 < z_S < 4.86$ .

*Ares*.- a mock galaxy cluster at  $z = 0.5$ , generated in a flat  $\Lambda$ CDM cosmological model with a matter density parameter  $\Omega_m = 0.272$ . It contains 242 multiple images from 85 sources (all with assumed known spectroscopic redshifts, spanning  $0.91 < z_S < 6.0$ ) and 330 cluster members. *Ares* is part of an archive of mock clusters which reproduce the characteristics of the *Frontier Fields* observations (the FF-SIMS Challenge, [Meneghetti et al. 2016](#)). It was part of a challenge among the strong lensing community to perform, first a blind reconstruction of the mass distribution of the cluster, and then to improve the models after the unblinding of the true mass distribution. The conclusions of this challenge were primarily used to calibrate different modeling techniques. *Ares* is a semi-analytical cluster created with MOKA<sup>4</sup> by [Giocoli et al. \(2012\)](#). This simulated cluster, a bimodal and realistic cluster, is built with three components: two smooth dark matter triaxial haloes, two bright central cluster galaxies (BCGs) and a large number of sub-haloes. Dark matter sub-haloes are populated using a Halo Occupation Distribution technique (HOD) and stellar and B-band luminosities are given for all galaxies according to the mass of their sub-halo as in [Wang et al. \(2006\)](#).

We have modeled *Ares* as two large-scale potentials and two potentials for the BCGs, whose coordinates are fixed as well as the ones for the large-scale potentials (see Figure 1 in [Acebron et al. 2017](#)). Both components have been parametrized with the PIEMD density profile and corresponds to the model PIEMD - PIEMD in [Acebron et al. \(2017\)](#). The modeling also includes cluster galaxies with  $m_{F160W} < 22$  (being a more complex cluster, computing time is reduced by introducing a magnitude cut representing  $> 90\%$  of the total cluster luminosity) with masses scaling with luminosity (see [Limousin et al. 2005](#), for further details). Three massive cluster galaxies close to multiple images (see Figure 1 in [Acebron et al. 2017](#)) were more carefully modeled (i.e their parameters deviate from the scaling relations).

<sup>4</sup> <https://cgiocoli.wordpress.com/research-interests/moka/>

All multiple images provided were taken into account in the modeling, resulting in an average positional accuracy of  $0.66''$  and giving tight constraints on the  $\Omega_M - w$  space parameter considering a flat  $\Lambda$ CDM cosmology .

To quantify how the cosmological constraints are biased due to systematic effects in the SL modeling, we use different image-positional errors,  $\delta_{pos}$ , and compare the resulting DE parameter estimations. For each parametric DE model and for both *Abell 1689* and *Ares*, we carry out three runs considering the following errors for the multiple images positions:  $0.25''$ ,  $0.5''$ , and  $1.0''$ . These values are arbitrary, but they intend to cover the range of values of the systematic errors reported by different authors (Zitrin et al. 2015; Harvey et al. 2016).

The best-fitting model parameters are found by minimizing the distance between the observed and model-predicted positions of the multiple images. To assess the goodness of the fit we examine the reduced chi-square  $\chi_{red}^2$  (see Jullo et al. 2007, for details how it is calculated in the source and image plane). We also use the root-mean-square between the observed and predicted positions of the multiple images from the modeling, computed as follows:

$$RMS = \sqrt{\frac{1}{N} \sum_{i=1}^n |\theta_i^{obs} - \theta_i^{pred}|^2}, \quad (19)$$

where  $\theta_i^{obs}$  and  $\theta_i^{pred}$  are the observed and model-predicted positions of the multiples images and N being the total number of images.

#### 4. RESULTS

In this section we present, for each cosmological model, the constraints from the strong lensing measurements of *Ares* and *Abell 1689*, as well as those from other complementary probes (H(z), SNe Ia, BAO, and CMB, see Appendix A). The mock *Ares* cluster has the advantage of being able to directly compare and validate the cosmological constraints from the SL technique with the fiducial cosmology.

For each cosmological model, the cluster model parameters and the cosmological parameters are simultaneously optimized with the LENSTOOL software with 80000 MCMC steps. For the complementary probes, we carry out the EMCEE python module (Foreman-Mackey et al. 2013) employing 500 walkers, 2500 burn-in phase steps, and 7500 MCMC steps to guaranty the convergence. In all our estimations, we have adopted a dimensionless Hubble constant  $h = 0.70$ .

Tables 1-5 show the mean parameters obtained after optimization for both *Abell 1689*, *Ares* and each cosmological model (JBP, BA, FSLL I, FSLL II, and SeLa). For each positional uncertainty considered, we present the  $\chi_{red}^2$ , the RMS in the image plane as well as the mean values obtained for the cosmological parameters fitted,  $\Omega_m$ ,  $w_0$  and  $w_1$  with the 68% uncertainties. The same Tables also give the mean values for the DE parameters obtained from the complementary probes.

##### 4.1. Effect of image-position error on the cosmological parameters

The positional error for the multiple images plays a key role in both the lens modeling and the cosmological parameter estimation (Limousin et al. 2016). We also note that the statistical estimators depend on the uncertainty considered for the position of the multiple images. As mentioned in §1, a large error could take into account other sources of uncertainties in the SL measurements, such as systematic errors due to foreground and background structures (D'Aloisio & Natarajan 2011; Host 2012; Bayliss et al. 2014; Zitrin et al. 2015) or the cluster's environment (McCully et al. 2017; Acebron et al. 2017). As a first test, we constrain the JBP cosmological parameters from *Ares* SL data with an image positional error  $\delta_{pos} = 1''$ . For this run (see Table 1), we obtain  $\chi_{red}^2 = 0.77$  and  $RMS = 0.94''$ , both criteria indicating a good-fit. When modeling *Ares* using smaller positional uncertainties ( $\delta_{pos} = 0.25'', 0.5''$ ), both the  $\chi_{red}^2$  and RMS values point out a poor model fit. The left panel of Figure 1 illustrates the comparison of the  $\Omega_m - w_0$  confidence contours obtained with the different positional uncertainties for the JBP model using *Ares* SL data. This Figure clearly shows that increasing the positional uncertainty is translated in an enlargement of the confidence contours and a systematic shift in the  $\Omega_{m0}$  estimation towards the fiducial value. Therefore, we confirm that more statistically significant constraints are obtained for larger errors, i.e., the reduced  $\chi_{red}^2$  value trending to one. This same trend is recovered for the BA, FSLL I, FSLL II and SeLa parameterizations (see Tables 2-5). Thus, in the following, we discuss the parameter estimation through SL modeling in *Abell 1689* using the largest error:  $\delta_{pos} = 1''$  (and compare it with smaller uncertainties as well).

##### 4.2. $w(z)$ parameter estimations from SL in *Abell 1689*

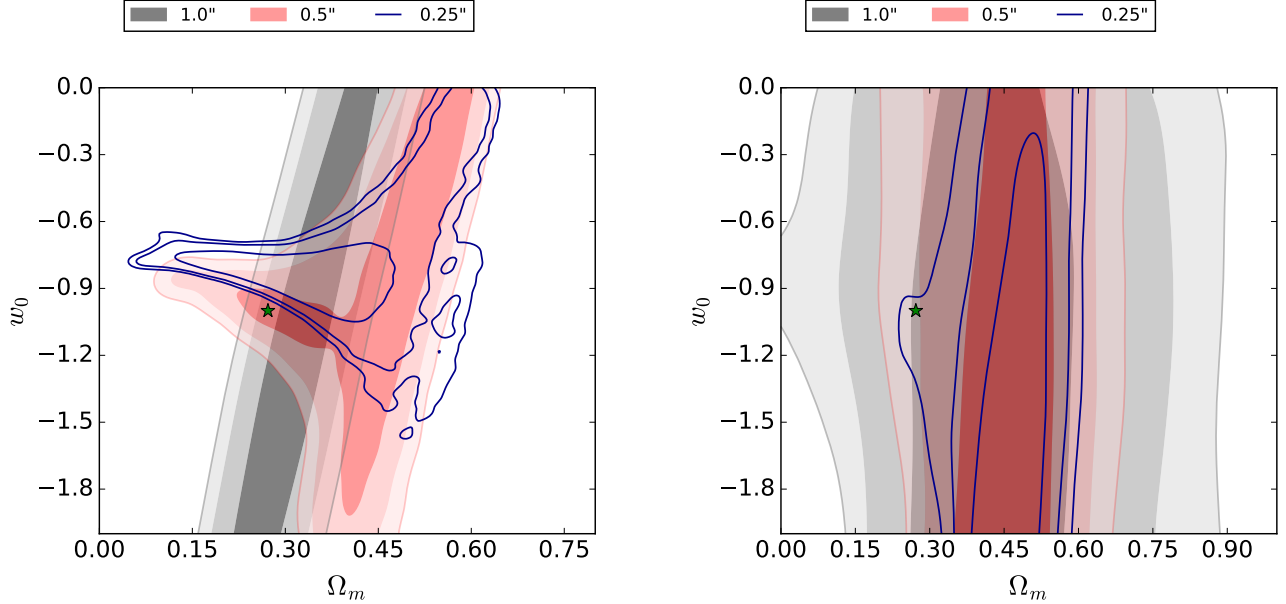


**Figure 1.** Comparison of the constraints on the  $\Omega_m$ - $w_0$  parameters for *Ares* (left panel) and *Abell1689* (right panel) when considering several positional uncertainties ( $\delta_{pos}$ ) in the SL modeling for the JBP parameters. The star indicates the reference values.

In general, for all models, we found that the SL technique using *Abell 1689* data provides better  $\Omega_m$  constraints than the ones on the equation of state parameters and confirm our previous result: a larger error ( $\delta_{pos} = 1''$ ) provides more significant constraints which is shown in the right panel of the Figure 1 for the JBP model. Furthermore, Figures 2-4 show the  $1\sigma$ ,  $2\sigma$ ,  $3\sigma$  confidence contours and the marginalized 1-dimensional posterior probability distributions on the  $\Omega_m$ ,  $w_0$ ,  $w_1$  parameters for the cosmological model JBP using *Abell 1689* SL data for each positional uncertainty considered. We note again that, when the error in the image position is increased, the  $\Omega_m$ - $w_0$  and  $\Omega_m$ - $w_1$  (or  $w_0$ - $w_1$ ) confidence contours shift towards the left (upper) region, where the confidence contours from BAO, CMB, SNe Ia, and  $H(z)$  probes are overlapped. This same trend is recovered for the BA, FSLL I, FSLL II and SeLa parameterizations (their confidence contours are provided in the Figs. B1-B4 of the Appendix B).

On the other hand, the  $w_0$  and  $w_1$  mean values for the five  $w(z)$  parameterizations could suggest a dynamical equation of state, which can be associated to thawing or freezing quintessence DE (Pantazis et al. 2016). Nevertheless, all our EoS constraints are consistent with the cosmological constant, i.e.  $w_0 = -1$ , and  $w_1 = 0$ , within the  $3\sigma$  confidence level. In addition, there is no significant difference among the  $\chi^2_{red}$  and RMS values for different  $w(z)$  parameterizations. Therefore, any parametric DE model could be the source of the late cosmic acceleration. We confirm this result in the left panel of the Figure 5 which show the reconstruction of the cosmological evolution for each parameterization using the mean values obtained from the SL modeling in *Abell 1689* when  $\delta_{pos} = 1''$  is considered.

#### 4.3. Deceleration parameter

The cosmological behavior of the deceleration parameter (Eq. 5) is an important test to know whether a DE model is able to handle the late cosmic acceleration. The right panels of Figure 5 shows the reconstructed  $q(z)$  evolution for each parameterization obtained from *Abell 1689* SL data when the multiple image-positional error is  $1''$ . We also have propagated its error within the  $1\sigma$  confidence level using a Monte Carlo approach. Notice that the five cosmological model predicts an accelerating expansion at late times. The transition redshifts, i.e. when the Universe passes from an decelerated phase to one accelerated, are  $z_t = 0.44^{+0.21}_{-0.17}, 0.44^{+0.17}_{-0.12}, 0.45^{+0.18}_{-0.13}, 0.50^{+0.22}_{-0.24}, 0.34^{+0.07}_{-0.04}$  for the JBP, BA, FSLL I, FSLL II, and SeLa parameterizations, respectively. Furthermore, the  $q(z)$  shape for each parameterization is consistent with that of the cosmological constant within the  $1\sigma$  confidence level.

## 5. CONCLUSIONS

Several recent studies have shown that dark energy could deviate from a cosmological constant (Ferreira et al. 2017; Zhao et al. 2017). A simple way to investigate such alternative dark energy models is to parameterize the dark energy

**Table 1.** JBP mean fit parameters obtained for both galaxy clusters SL data. The columns give the reduced  $\chi_{red}^2$ , RMS in the image plane (in arcseconds) and the mean values for  $\Omega_m$ ,  $w_0$ ,  $w_1$  with 68% confidence level errors. The mean values estimated with H(z), SNIa, BAO and CMB data are also provided.

Cluster name	Error in the pos. (")	$\chi_{red}^2$	RMS (")	$\Omega_m$	$w_0$	$w_1$
Abell 1689	0.25	11.37	0.54	$0.47_{-0.06}^{+0.04}$	$-1.29_{-0.01}^{+1.04}$	$-6.46_{-0.33}^{+4.88}$
<i>Ares</i>		2.73	0.59	$0.37_{-0.11}^{+0.12}$	$-0.82_{-0.11}^{+0.11}$	$-0.14_{-0.04}^{+0.36}$
Abell 1689	0.5	3.14	0.64	$0.46_{-0.08}^{+0.08}$	$-1.11_{-0.04}^{+1.20}$	$-6.14_{-0.07}^{+5.49}$
<i>Ares</i>		0.78	0.65	$0.46_{-0.11}^{+0.06}$	$-0.90_{-0.49}^{+0.60}$	$-1.77_{-3.01}^{+0.07}$
Abell 1689	1.0	0.95	0.88	$0.43_{-0.12}^{+0.18}$	$-1.07_{-0.60}^{+0.69}$	$-5.09_{-3.40}^{+3.07}$
<i>Ares</i>		0.77	0.94	$0.33_{-0.06}^{+0.06}$	$-1.06_{-0.43}^{+0.83}$	$-5.81_{-3.16}^{+3.41}$
Complementary probes						
H(z)	—	0.54	—	$0.26_{-0.02}^{+0.01}$	$-0.88_{-0.19}^{+0.27}$	$-0.70_{-2.59}^{+1.83}$
SNIa	—	0.98	—	$0.32_{-0.10}^{+0.05}$	$-0.70_{-0.18}^{+0.19}$	$-4.44_{-3.49}^{+3.40}$
BAO	—	2.17	—	$0.25_{-0.02}^{+0.02}$	$-1.34_{-0.15}^{+0.26}$	$0.43_{-1.99}^{+1.13}$
CMB	—	58.8	—	$0.32_{-0.002}^{+0.002}$	$-0.69_{-0.68}^{+0.50}$	$-4.54_{-3.66}^{+4.26}$

**Table 2.** The same as Table 1 for the BA parameterization.

Cluster name	Error in the pos. (")	$\chi_{red}^2$	RMS (")	$\Omega_m$	$w_0$	$w_1$
Abell 1689	0.25"	11.40	0.54	$0.47_{-0.06}^{+0.05}$	$-1.32_{-0.01}^{+0.98}$	$-6.28_{-0.07}^{+5.31}$
<i>Ares</i>		2.69	0.59	$0.27_{-0.01}^{+0.46}$	$-0.89_{-0.48}^{+0.16}$	$0.09_{-1.10}^{+0.91}$
Abell 1689	0.5"	3.15	0.64	$0.44_{-0.10}^{+0.08}$	$-1.15_{-0.02}^{+1.20}$	$-5.22_{-0.57}^{+6.17}$
<i>Ares</i>		0.80	0.65	$0.20_{-0.01}^{+0.36}$	$-1.10_{-0.24}^{+0.31}$	$0.36_{-1.81}^{+0.16}$
Abell 1689	1.0"	0.94	0.89	$0.41_{-0.15}^{+0.17}$	$-1.08_{-0.02}^{+1.26}$	$-4.49_{-7.69}^{+0.62}$
<i>Ares</i>		0.33	0.93	$0.26_{-0.0}^{+0.31}$	$-1.37_{-0.24}^{+0.31}$	$-1.88_{-6.28}^{+0.18}$
Complementary probes						
H(z)	—	0.57	—	$0.25_{-0.08}^{+0.02}$	$-0.90_{-0.12}^{+0.13}$	$0.01_{-0.85}^{+0.43}$
SNIa	—	0.98	—	$0.37_{-0.09}^{+0.04}$	$-0.78_{-0.17}^{+0.22}$	$-3.24_{-3.14}^{+2.37}$
BAO	—	2.25	—	$0.26_{-0.02}^{+0.02}$	$-1.23_{-0.16}^{+0.18}$	$-0.23_{-0.69}^{+0.52}$
CMB	—	58.8	—	$0.32_{-0.002}^{+0.002}$	$-0.63_{-0.67}^{+0.45}$	$-2.24_{-1.82}^{+2.18}$

equation of state as a function of redshift. In order to elucidate the nature of dark energy, numerous parameterizations have been proposed (see for instance [Pantazis et al. 2016](#), and references therein). The typical tests to constrain cosmological parameters use SNe Ia, H(z), BAO and CMB distance posterior measurements. Nevertheless, some of them could provide biased constraints because either the data or the test fitting formulae are derived assuming an underlying standard cosmology (see Appendix A). Furthermore, new complementary techniques could break the degeneracy between parameters and obtain stringent constraints which could help us distinguish the nature of dark energy.

In this paper, which is the first in a series, we investigate a promising technique to study alternative cosmological models and to constrain their parameters using the strong lensing measurements in galaxy clusters. This method has the advantage of providing constraints which are not biased due to an underlying cosmology.

We have considered the following five popular bi-parametric CPL-like ansatz: JBP, BA, FSLL I, FSLL II, and SeLa and constrained their parameters using the SL data in a real galaxy cluster, *Abell 1689*, and a simulated one *Ares*. We

**Table 3.** The same as Table 1 for the FSSL I parameterization.

Cluster name	Error in the pos. (")	$\chi_{red}^2$	RMS (")	$\Omega_m$	$w_0$	$w_1$
Abell 1689	0.25"	11.53	0.54	$0.46^{+0.05}_{-0.06}$	$-1.39^{+0.93}_{-0.04}$	$-6.60^{+5.04}_{-0.07}$
<i>Ares</i>		2.70	0.59	$0.17^{+0.22}_{-0.03}$	$-0.99^{+0.24}_{-0.16}$	$0.48^{+0.29}_{-0.72}$
Abell 1689	0.5"	3.07	0.64	$0.42^{+0.09}_{-0.12}$	$-1.17^{+1.08}_{-0.21}$	$-4.75^{+0.14}_{-8.73}$
<i>Ares</i>		0.80	0.65	$0.23^{+0.36}_{-0.02}$	$-1.36^{+0.60}_{-0.15}$	$0.79^{+0.08}_{-3.00}$
Abell 1689	1.0"	0.93	0.89	$0.40^{+0.17}_{-0.15}$	$-1.15^{+1.07}_{-0.16}$	$-4.99^{+6.08}_{-1.12}$
<i>Ares</i>		0.33	0.92	$0.27^{+0.32}_{-0.01}$	$-1.45^{+0.97}_{-0.15}$	$-1.89^{+0.13}_{-7.13}$
Complementary probes						
H(z)	—	0.48	—	$0.25^{+0.02}_{-0.06}$	$-0.95^{+0.19}_{-0.15}$	$0.14^{+1.03}_{-1.46}$
SNIa	—	0.98	—	$0.36^{+0.05}_{-0.10}$	$-0.74^{+0.22}_{-0.18}$	$-3.77^{+2.77}_{-3.37}$
BAO	—	2.13	—	$0.24^{+0.02}_{-0.02}$	$-1.40^{+0.25}_{-0.19}$	$0.51^{+0.92}_{-1.24}$
CMB	—	58.8	—	$0.32^{+0.002}_{-0.002}$	$-0.69^{+0.50}_{-0.68}$	$-2.86^{+3.05}_{-2.54}$

**Table 4.** The same as Table 1 for the FSSL II parameterization.

Cluster name	Error in the pos. (")	$\chi_{red}^2$	RMS (")	$\Omega_m$	$w_0$	$w_1$
Abell 1689	0.25"	11.90	0.54	$0.41^{+0.05}_{-0.06}$	$-1.61^{+0.54}_{-0.03}$	$-5.59^{+6.82}_{-0.09}$
<i>Ares</i>		2.71	0.59	$0.19^{+0.33}_{-0.01}$	$-0.81^{+0.06}_{-0.10}$	$0.18^{+0.13}_{-0.80}$
Abell 1689	0.5"	3.17	0.64	$0.38^{+0.09}_{-0.10}$	$-1.45^{+0.57}_{-0.26}$	$-4.81^{+7.24}_{-0.29}$
<i>Ares</i>		0.79	0.65	$0.38^{+0.15}_{-0.21}$	$-1.00^{+0.25}_{-0.44}$	$-0.64^{+0.38}_{-4.69}$
Abell 1689	1.0"	0.94	0.89	$0.35^{+0.20}_{-0.14}$	$-1.29^{+0.70}_{-0.31}$	$-4.78^{+7.57}_{-0.10}$
<i>Ares</i>		0.32	0.92	$0.28^{+0.06}_{-0.14}$	$-1.35^{+0.29}_{-0.54}$	$-2.11^{+0.50}_{-7.14}$
Complementary probes						
H(z)	—	0.56	—	$0.26^{+0.02}_{-0.06}$	$-0.92^{+0.11}_{-0.10}$	$-0.30^{+0.92}_{-2.12}$
SNIa	—	0.98	—	$0.32^{+0.04}_{-0.11}$	$-0.98^{+0.15}_{-0.15}$	$-4.34^{+3.90}_{-3.86}$
BAO	—	2.21	—	$0.27^{+0.02}_{-0.02}$	$-1.19^{+0.12}_{-0.10}$	$-1.34^{+1.23}_{-1.91}$
CMB	—	58.8	—	$0.32^{+0.002}_{-0.002}$	$-0.87^{+0.22}_{-0.34}$	$-4.96^{+4.01}_{-3.51}$

implemented these  $w(z)$  parameterizations in the LENSTOOL code which uses a MCMC algorithm to simultaneously constrain the lens model and the  $w(z)$  parameters. In addition, we have considered three different image-positional errors to quantify how the cosmological constraints are affected by these uncertainties in the lens modeling. In general, we found that the SL technique provides competitive constraints on the  $w(z)$  parameters in comparison with the common cosmological tests. Moreover, when increasing the image-positional error (from 0.5" to 1.0"), we find that systematic biases with respect to the known input cosmological values in the simulated cluster decrease. After taking this calibration into account in the real data, our SL constraints are consistent with those obtained from other probes.

In summary, we have exploited the strong lensing modeling in galaxy clusters as a cosmological probe. Although we have measured competitive constraints on the  $w(z)$  parameters, further analysis on the galaxy clusters and their environment is needed to improve the strong lensing modeling and hence to more tightly estimate cosmological parameters. In forthcoming papers, we will test this method to constrain the parameter of other cosmological scenarios, for instance, those considering interactions in the dark sector.

**Table 5.** The same as Table 1 for the SeLa parameterization.

Cluster name	Error in the pos. (")	$\chi_{red}^2$	RMS (")	$\Omega_m$	$w_0$	$w_{0.5}$
Abell 1689	0.25"	11.66	0.54	$0.42^{+0.07}_{-0.10}$	$-1.23^{+0.94}_{-0.24}$	$0.61^{+0.38}_{-1.57}$
<i>Ares</i>		6.01	4.80	$0.80^{+0.06}_{-0.09}$	$-1.04^{+1.25}_{-0.08}$	$0.38^{+0.65}_{-1.56}$
Abell 1689	0.5"	3.06	0.64	$0.41^{+0.11}_{-0.09}$	$-1.18^{+1.06}_{-0.13}$	$-0.54^{+0.02}_{-1.96}$
<i>Ares</i>		1.57	1.11	$0.66^{+0.12}_{-0.09}$	$-1.26^{+1.07}_{-0.01}$	$-0.59^{+0.14}_{-1.83}$
Abell 1689	1.0"	0.93	0.90	$0.46^{+0.04}_{-0.05}$	$-1.39^{+0.73}_{-0.44}$	$-6.60^{+3.87}_{-2.44}$
<i>Ares</i>		0.48	1.06	$0.41^{+0.16}_{-0.10}$	$-1.16^{+1.17}_{-0.04}$	$0.49^{+0.79}_{-1.40}$
Complementary probes						
H(z)	—	0.55	—	$0.25^{+0.02}_{-0.07}$	$-0.90^{+0.14}_{-0.12}$	$-1.01^{+0.31}_{-0.36}$
SNIa	—	0.98	—	$0.37^{+0.05}_{-0.09}$	$-0.73^{+0.28}_{-0.18}$	$-2.64^{+1.23}_{-1.57}$
BAO	—	9.95	—	$0.23^{+0.04}_{-0.08}$	$-1.04^{+0.28}_{-0.23}$	$-1.11^{+0.55}_{-0.37}$
CMB	—	58.8	—	$0.32^{+0.002}_{-0.002}$	$-0.56^{+0.40}_{-0.54}$	$-1.98^{+0.51}_{-0.50}$

LAM staff where part of this work was done. This work has been carried out thanks to the support of the OCEVU Labex (ANR-11-LABX-0060) and the A\*MIDEX project (ANR-11-IDEX-0001-02) funded by the "Investissements d'Avenir" French government program managed by the ANR.

This work was granted access to the HPC resources of Aix-Marseille Université financed by the project Equip@Meso (ANR-10-EQPX-29-01) of the program "Investissements d'Avenir" supervised by the Agence Nationale pour la Recherche. This research has been carried out thanks to PROGRAMA UNAM-DGAPA-PAPIIT IA102517. T. V. thanks the staff of the Instituto de Física y Astronomía of the Universidad de Valparaíso. M.L. acknowledges the support from Centre national de la recherche scientifique (CNRS) & Programme National de Cosmologie et Galaxies (PNCG).

## APPENDIX

### A. ADDITIONAL COSMOLOGICAL DATA

We compare the constraints obtained from the strong lensing modeling with those from BAO, CMB, SNe Ia and H(z) cosmological probes. In the following we describe briefly these cosmological data, for further details on how their figure-of-merit is constructed see [Magaña et al. \(2015\)](#); [Magaña et al. \(2017\)](#) and references therein.

#### A.1. BAO

Large-scale galaxy surveys offer the possibility of measuring the signature of Baryon Acoustic Oscillations which is a typical length scale imprinted in both photons and baryons by the propagation of sound waves in the primordial plasma of the Universe. This signal, i.e. the sound horizon at the drag epoch,  $r_s(z_d)$ , is a standard ruler which can be used to test alternative cosmologies. To complement our SL constraints, we use the following 9 BAO points (see [Magaña et al. 2017](#), and references therein) to constrain the  $w(z)$  functions:

- 6dFGS.-  $z = 0.106$ ,  $dz \equiv \frac{r_s(z_d)}{D_V(z)} = 0.336 \pm 0.015$ , where  $D_V(z) = \frac{1}{H_0} \left[ (1+z)^2 D(z)^2 \frac{cz}{E(z)} \right]^{1/3}$
- WiggleZ.-  $z = [0.44, 0.6, 0.73]$ ,  $dz = [0.0870 \pm 0.0042, 0.0672 \pm 0.0031, 0.0593 \pm 0.0020]$
- SDSS DR7  $z = 0.15$ ,  $0.2239 \pm 0.0084$
- SDSS-III BOSS DR11 (a).-  $z = [0.32, 57]$ ,  $dz = [0.1181 \pm 0.0022, 0.0726 \pm 0.0007]$
- SDSS-III BOSS DR11 (b).-  $z = [2.34, 2.36]$ ,  $\frac{D_H(z)}{r_s(z_d)} = [9.18 \pm 0.28, 9.00 \pm 0.3]$ , where  $D_H(z) = c/H_0 E(z)$

It is worth noting that  $r_s(z_d)$  depends on the underlying cosmology which is commonly the  $\Lambda$ CDM model. Moreover, the  $z_d$  formulae employed in the BAO fitting ([Eisenstein & Hu 1998](#)) were calculated for the standard cosmology. Thus, the BAO constraints could be biased due to the standard cosmology.

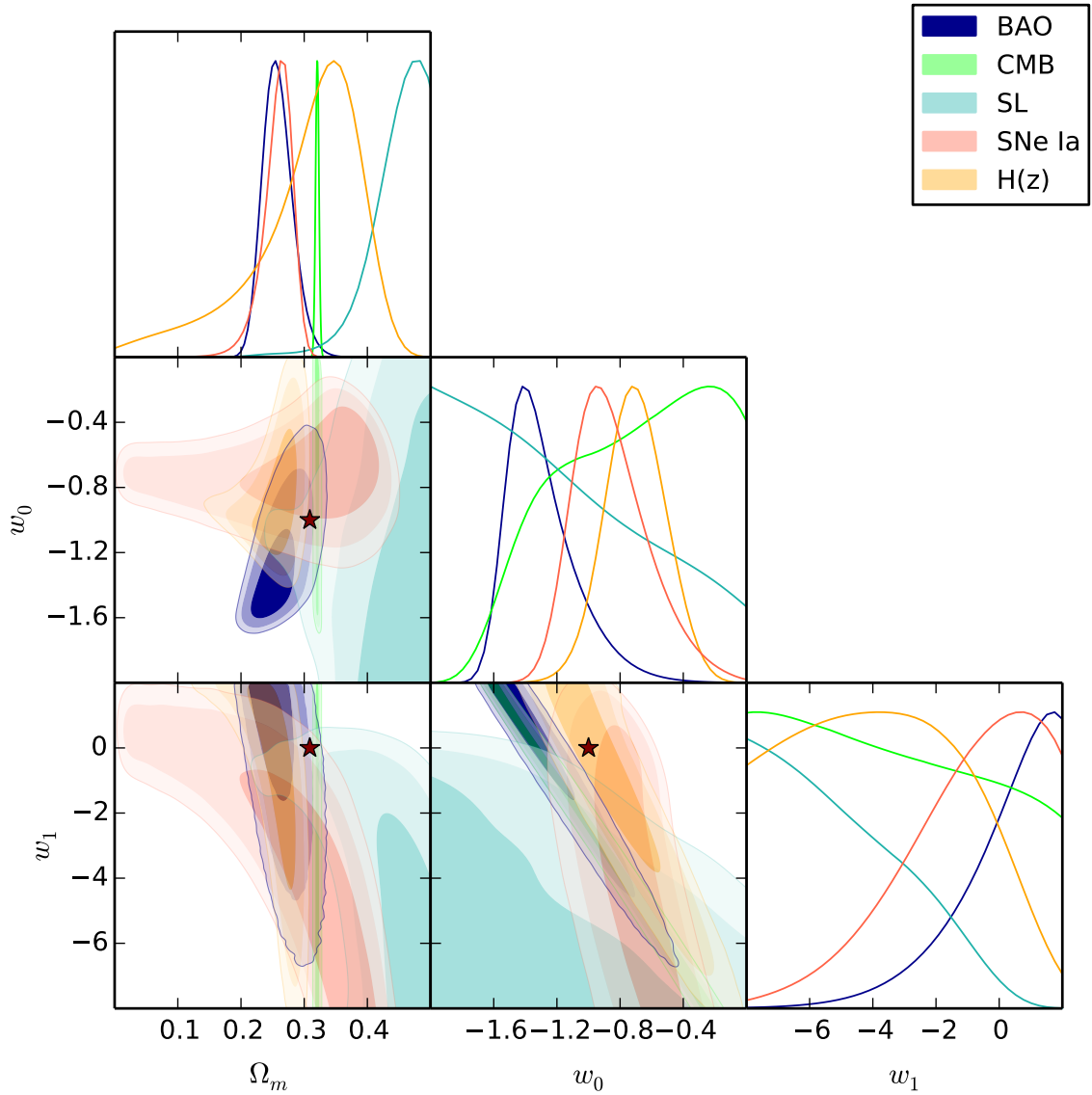


**Figure 2.** Confidence contours ( $1\sigma$ ,  $2\sigma$ ,  $3\sigma$ ) and the marginalized 1-dimensional posterior probability distributions on the  $\Omega_m$ ,  $w_0$  and  $w_1$  parameters for the cosmological model JBP for Abell 1689 with  $\delta_{pos} = 0.25''$ . The star indicates the cosmological parameters as constrained by [Planck Collaboration et al. \(2016b\)](#).

### A.2. Distance posteriors from CMB Planck 2015 measurements

The information of the CMB acoustic peaks can be compressed in three quantities, their distance posteriors: the acoustic scale,  $l_A$ , the shift parameter,  $R$ , and the decoupling redshift,  $z_*$ . Several authors have proved that these quantities are almost independent of the input DE models ([Wang et al. 2012](#)). Thus, to constrain the  $w(z)$  parameters we use the following distance posteriors for a flat  $w$ CDM, estimated by [Neveu et al. \(2017\)](#) from Planck 2015 measurements:  $l_A^{obs} = 301.787 \pm 0.089$ ,  $R^{obs} = 1.7492 \pm 0.0049$ ,  $z_*^{obs} = 1089.99 \pm 0.29$ .

It is worth noting that the fitting formulae for these quantities ([Hu & Sugiyama 1996](#); [Bond et al. 1997](#)) are calculated for the standard model, however we assume that they are valid in dynamical DE models.

### A.3. SNe Ia

Since that Type Ia Supernovae are standard candles, i.e. their light curves have the same shape after a standardization process, they have been used to measure cosmological parameters. Indeed, the apparent cosmic accelerating expansion was observed through a Hubble diagram of distant SNIa. As complementary test, we consider the compilation by [Ganeshalingam et al. \(2013\)](#) which contains 586 data points of the modulus distance,  $\mu$ , in the redshift range  $0.01 < z < 1.4$  which include mainly 91 points from the Lick Observatory Supernova Search (LOSS) SN Ia observations.

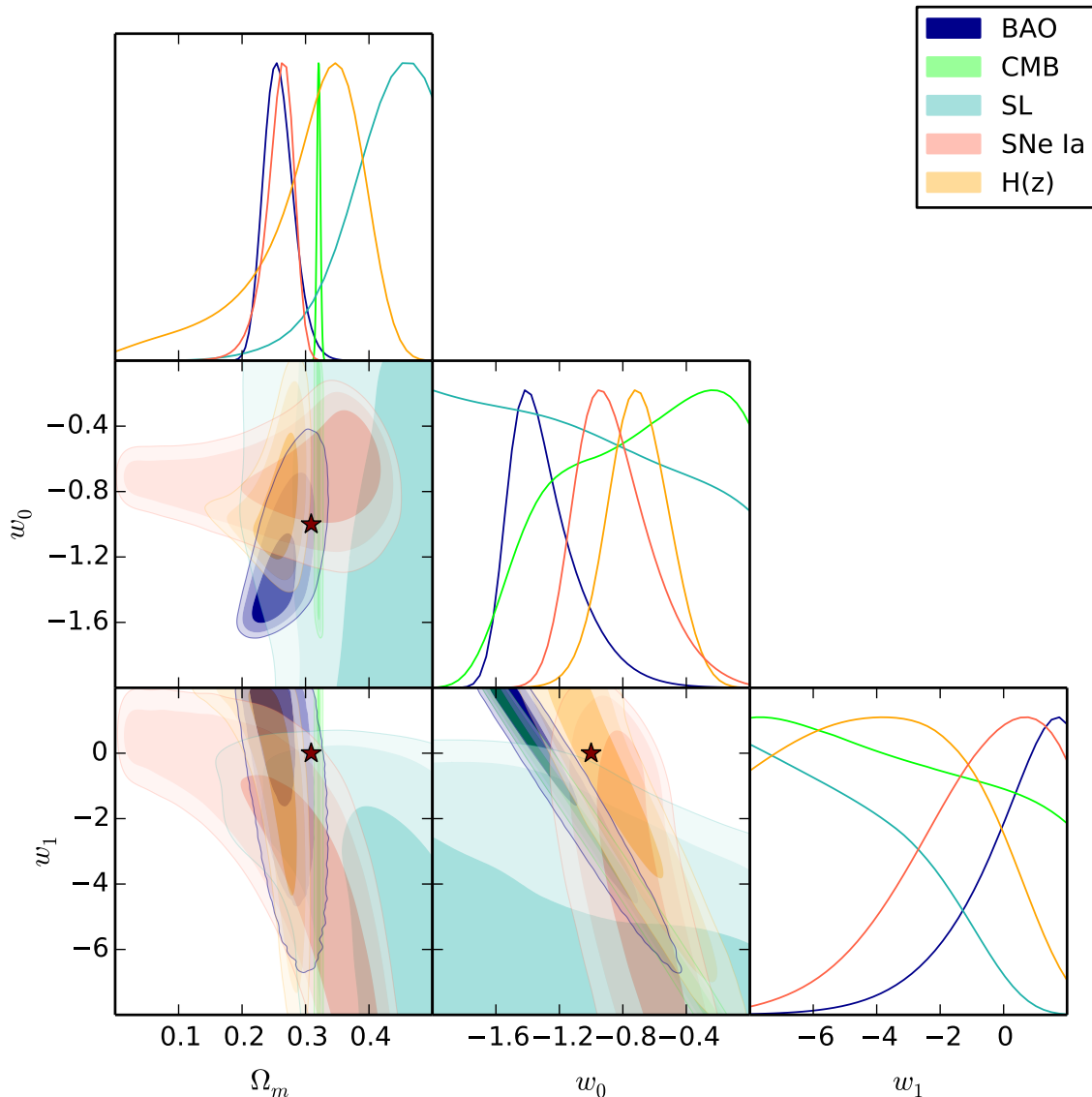


**Figure 3.** Confidence contours ( $1\sigma$ ,  $2\sigma$ ,  $3\sigma$ ) and the marginalized 1-dimensional posterior probability distributions on the  $\Omega_m$ ,  $w_0$  and  $w_1$  parameters for the cosmological model JBP for Abell 1689 with  $\delta_{pos} = 0.5''$ . The star indicates the cosmological parameters as constrained by [Planck Collaboration et al. \(2016b\)](#).

#### A.4. $H(z)$ measurements

The Hubble parameter at different redshifts provide a direct measurement of the expansion rate of the Universe. Several authors have estimated the observational Hubble data using different techniques: from clustering or BAO peaks (see for instance, [Gaztanaga et al. 2009](#)) and from cosmic chronometers ([Jimenez & Loeb 2002](#)). Here, we use the same sample used by [Magaña et al. \(2017\)](#) which contains 34 data points in the redshift range  $0.07 < z < 2.36$ . Although some of the  $H(z)$  points were estimated from BAO data, we assume that there is no correlation between them. It is worth noting that the  $H(z)$  points obtained from BAO could yield to biased constraints due to the underlying ( $\Lambda$ CDM) cosmology on  $r_s(z_d)$ .

## B. CONFIDENCE CONTOURS FOR THE BA, FSLL I, FSLL II AND SELA PARAMETERIZATIONS

### REFERENCES

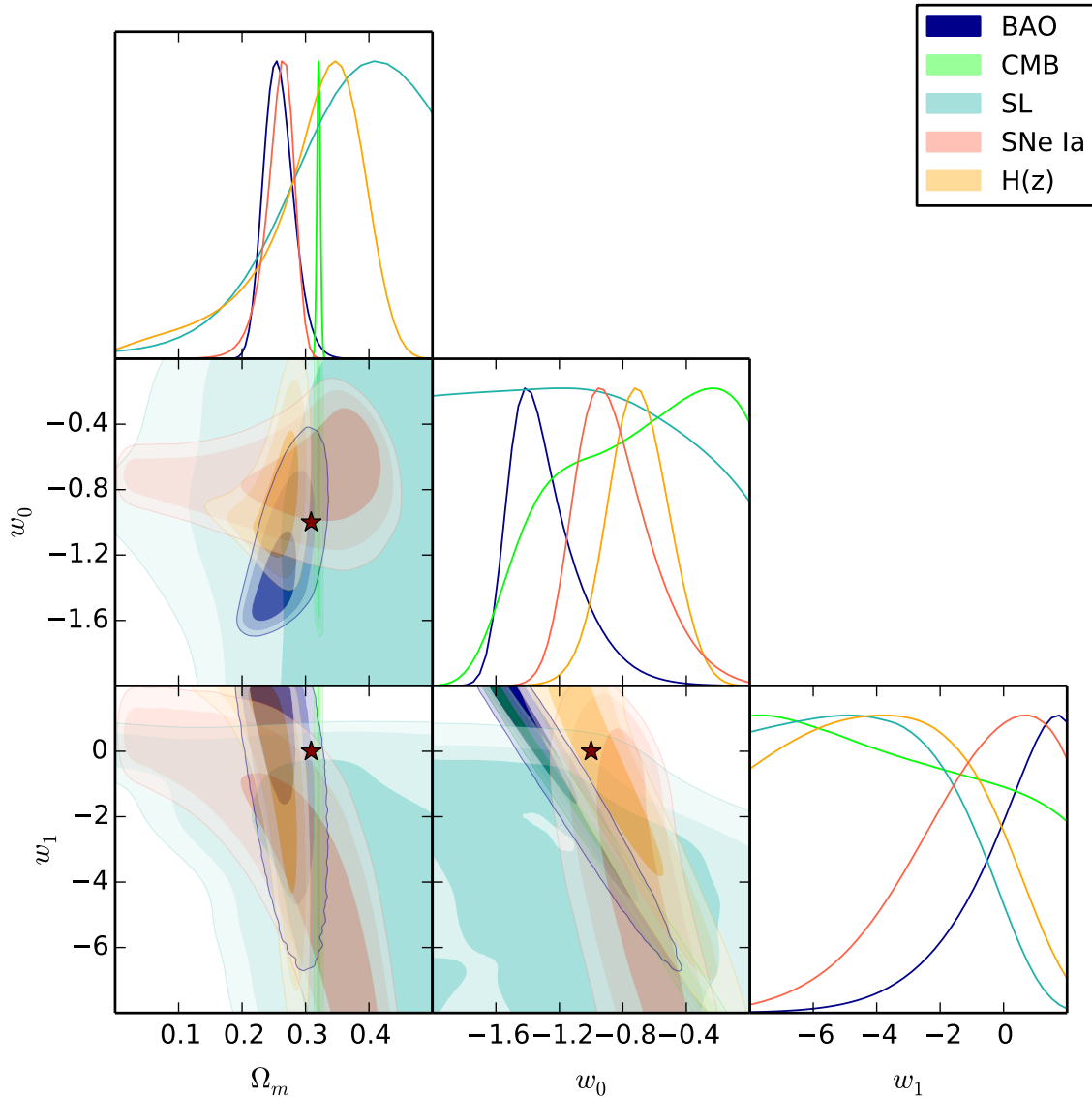


**Figure 4.** Confidence contours ( $1\sigma$ ,  $2\sigma$ ,  $3\sigma$ ) and the marginalized 1-dimensional posterior probability distributions on the  $\Omega_m$ ,  $w_0$  and  $w_1$  parameters for the cosmological model JBP for Abell 1689 with  $\delta_{pos} = 1.0''$ . The star indicates the cosmological parameters as constrained by [Planck Collaboration et al. \(2016b\)](#).

Bayliss, M. B., Johnson, T., Gladders, M. D., Sharon, K., & Oguri, M. 2014, *ApJ*, 783, 41  
 Bina, D., Pelló, R., Richard, J., et al. 2016, *A&A*, 590, A14  
 Bond, J. R., Efstathiou, G., & Tegmark, M. 1997, *MNRAS*, 291, L33  
 Caminha, G. B., Grillo, C., Rosati, P., et al. 2016, *A&A*, 587, A80  
 Chevallier, M., & Polarski, D. 2001, *International Journal of Modern Physics D*, 10, 213  
 Copeland, E. J., Sami, M., & Tsujikawa, S. 2006, *International Journal of Modern Physics D*, 15, 1753  
 D’Aloisio, A., & Natarajan, P. 2011, *MNRAS*, 411, 1628  
 Davis, T. M. 2014, *General Relativity and Gravitation*, 46, 1731  
 Diego, J. M., Broadhurst, T., Benitez, N., et al. 2015, *MNRAS*, 446, 683  
 Eisenstein, D. J., & Hu, W. 1998, *ApJ*, 496, 605  
 Elíasdóttir, Á., Limousin, M., Richard, J., et al. 2007, *ArXiv e-prints*, arXiv:0710.5636

Feng, C.-J., Shen, X.-Y., Li, P., & Li, X.-Z. 2012, *JCAP*, 9, 023  
 Ferreira, E. G. M., Quintin, J., Costa, A. A., Abdalla, E., & Wang, B. 2017, *Phys. Rev. D*, 95, 043520  
 Foreman-Mackey, D., Hogg, D. W., Lang, D., & Goodman, J. 2013, *PASP*, 125, 306  
 Ganeshalingam, M., Li, W., & Filippenko, A. V. 2013, *MNRAS*, 433, 2240  
 Gaztanaga, E., Cabre, A., & Hui, L. 2009, *Mon. Not. Roy. Astron. Soc.*, 399, 1663  
 Giocoli, C., Bonamigo, M., Limousin, M., et al. 2016, *MNRAS*, 462, 167  
 Giocoli, C., Meneghetti, M., Bartelmann, M., Moscardini, L., & Boldrin, M. 2012, *MNRAS*, 421, 3343  
 Golse, G., Kneib, J.-P., & Soucaill, G. 2002, *A&A*, 387, 788  
 Harvey, D., Kneib, J. P., & Jauzac, M. 2016, *MNRAS*, 458, 660  
 Host, O. 2012, *MNRAS*, 420, L18  
 Hu, W., & Sugiyama, N. 1996, *ApJ*, 471, 542

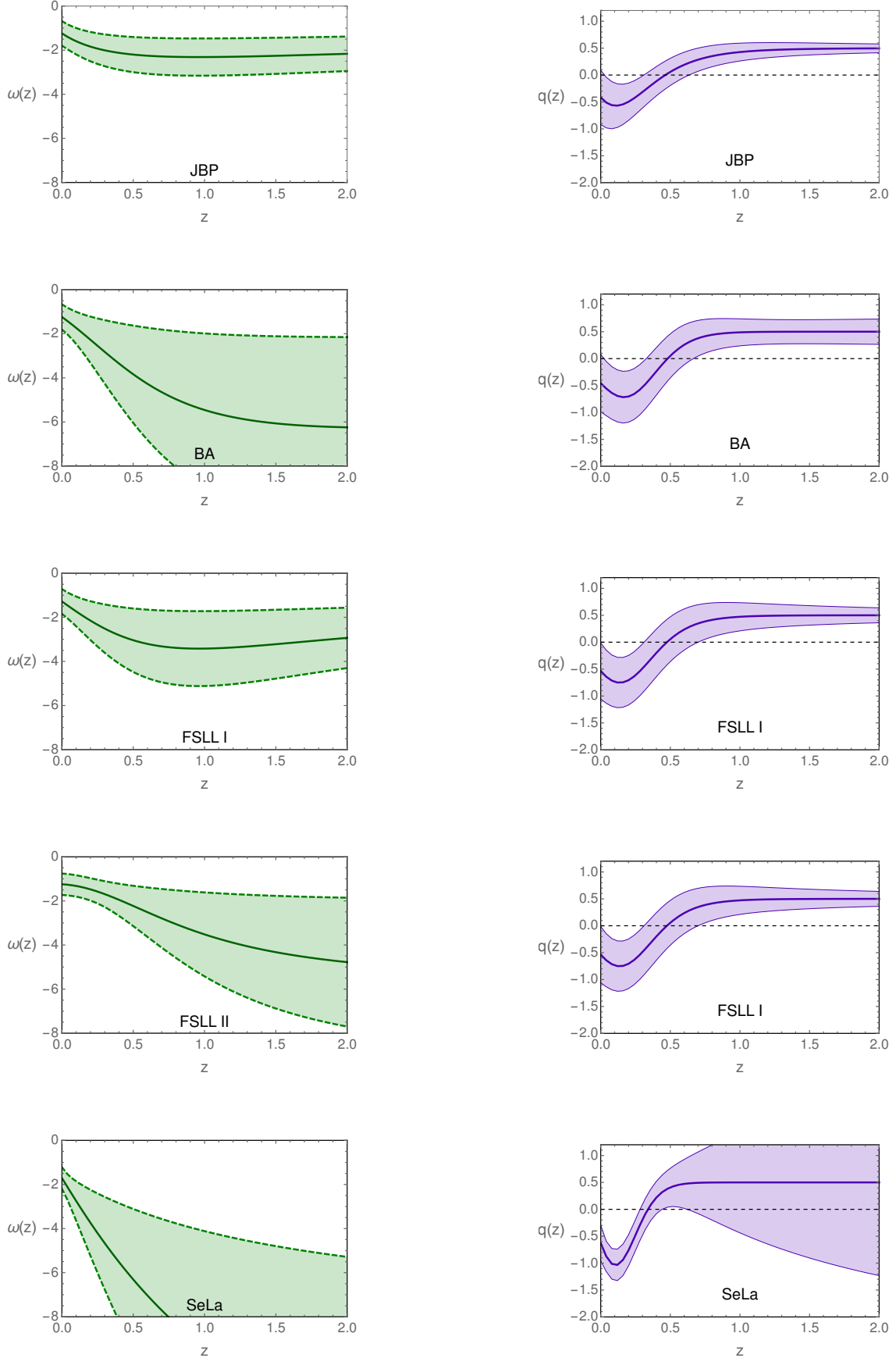


**Figure 5.** Reconstructed equation of state (left panel) and deceleration parameter (right panel) vs. redshift for each  $w(z)$  parameterization using the mean values obtained from SL data in *Abell 1689* with an image-position error of  $1.0''$ . The shadow regions show the  $1\sigma$  region calculated with a MCMC error propagation approach using the SL posterior constraints.

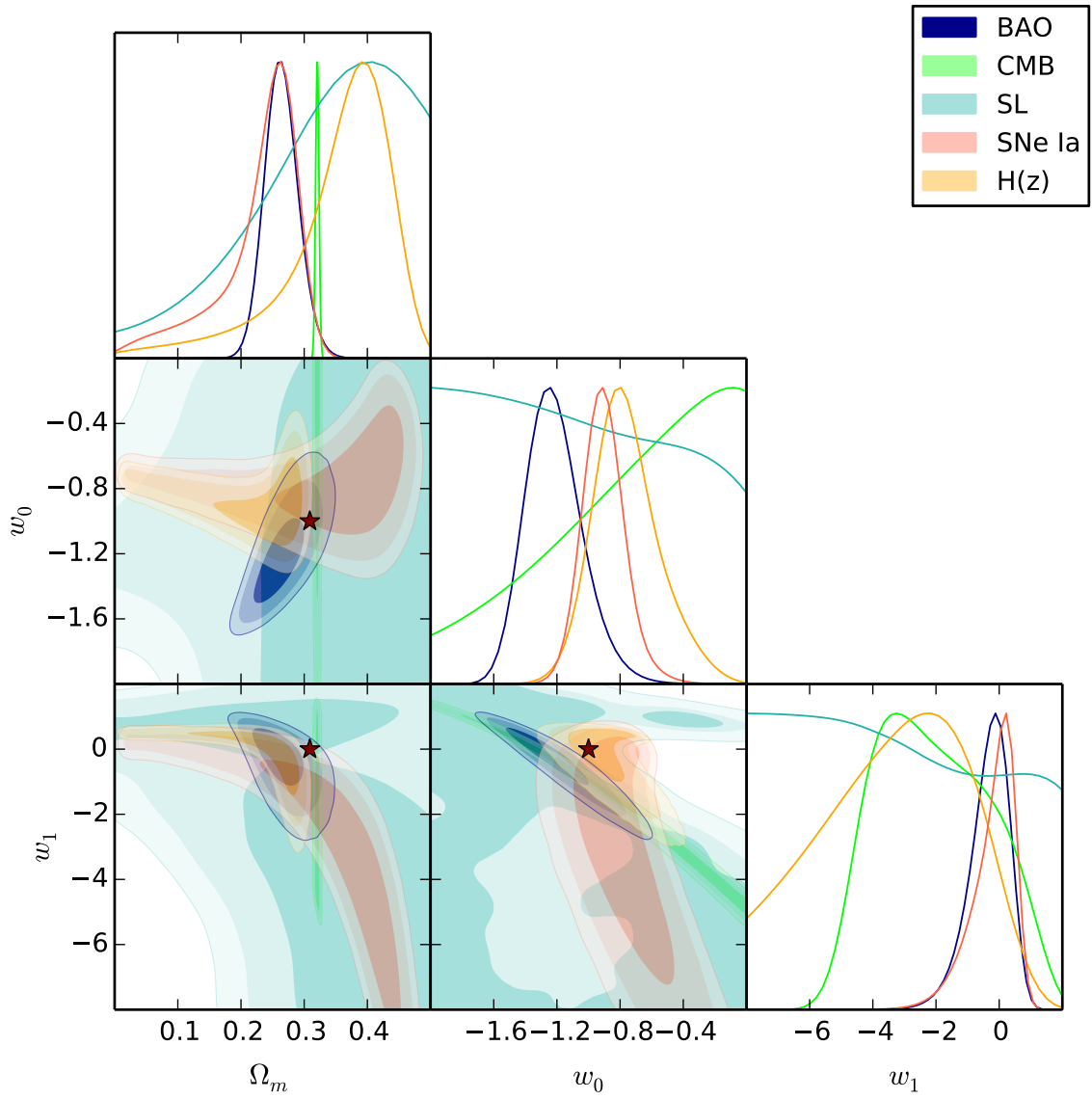


**Figure B1.** The same as Fig. 4 for the BA parameterization.

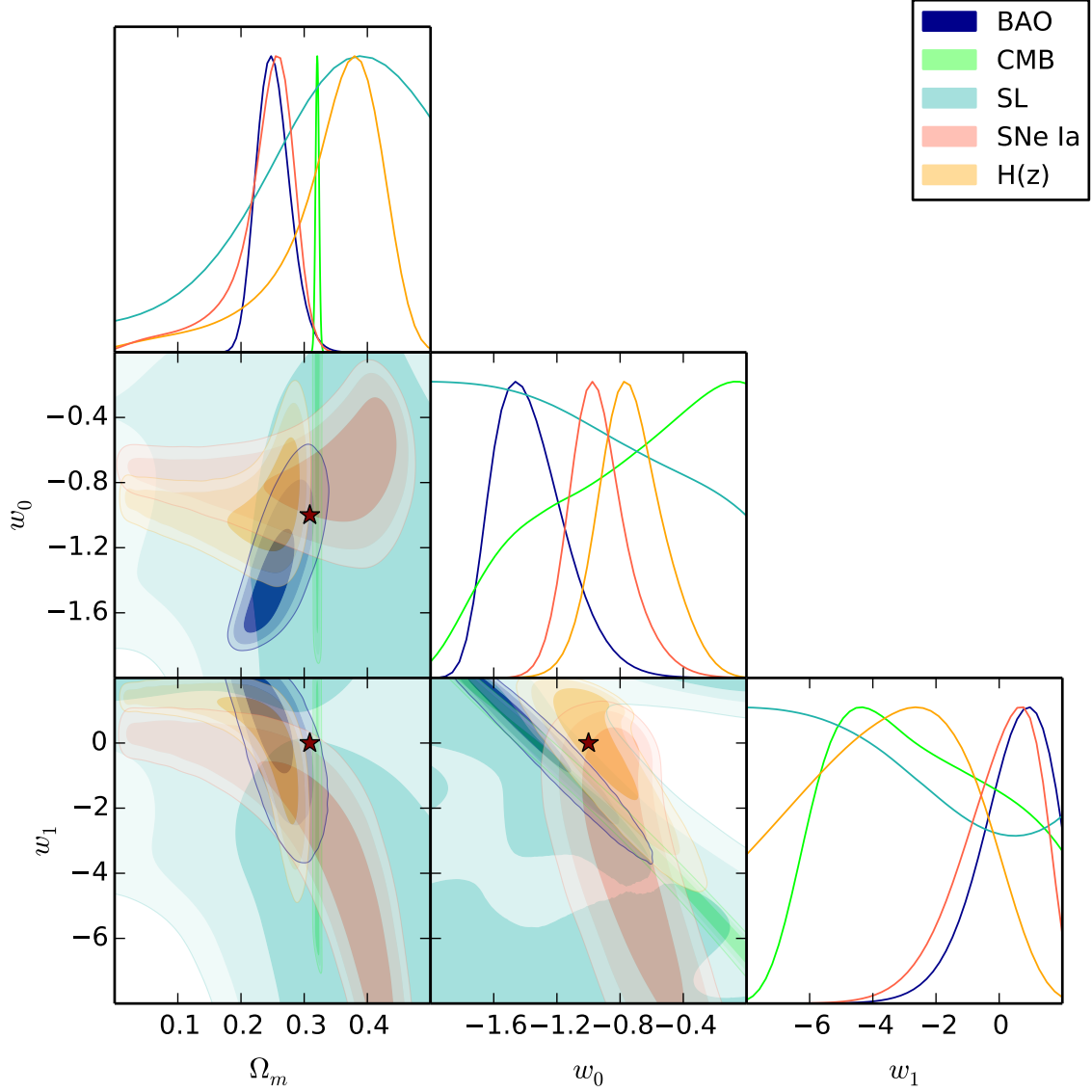


**Figure B2.** The same as Fig. 4 for the FSSL I parameterization.

Jaroszynski, M., & Kostrzewa-Rutkowska, Z. 2014, *MNRAS*, 439, 2432  
 Jassal, H. K., Bagla, J. S., & Padmanabhan, T. 2005a, *PhRvD*, 72, 103503  
 —. 2005b, *MNRAS*, 356, L11  
 Jauzac, M., Clément, B., Limousin, M., et al. 2014, *MNRAS*, 443, 1549  
 Jimenez, R., & Loeb, A. 2002, *Astrophys. J.*, 573, 37  
 Joyce, A., Lombriser, L., & Schmidt, F. 2016, *Annual Review of Nuclear and Particle Science*, 66, 95  
 Jullo, E., Kneib, J.-P., Limousin, M., et al. 2007, *MNRAS*, 9, 447  
 Jullo, E., Natarajan, P., Kneib, J.-P., et al. 2010, *Science*, 329, 924  
 Kassiola, A., & Kovner, I. 1993, *ApJ*, 417, 450  
 Kneib, J.-P., Ellis, R. S., Smail, I., Couch, W. J., & Sharples, R. M. 1996, *ApJ*, 471, 643  
 Komatsu, E., et al. 2011, *Astrophys. J. Suppl.*, 192, 18  
 Lazkoz, R., Nesseris, S., & Perivolaropoulos, L. 2005, *JCAP*, 11, 010

Li, M., Li, X.-D., Wang, S., & Wang, Y. 2011, *Communications in Theoretical Physics*, 56, 525  
 Limousin, M., Kneib, J.-P., & Natarajan, P. 2005, *MNRAS*, 356, 309  
 Limousin, M., Morandi, A., Sereno, M., et al. 2013, *SSRv*, 177, 155  
 Limousin, M., Richard, J., Jullo, E., et al. 2007, *ApJ*, 668, 643  
 Limousin, M., Jullo, E., Richard, J., et al. 2010, *A&A*, 524, A95  
 Limousin, M., Richard, J., Jullo, E., et al. 2016, *A&A*, 588, A99  
 Linder, E. V. 2003, *Physical Review Letters*, 90, 091301  
 Link, R., & Pierce, M. J. 1998, *ApJ*, 502, 63  
 Magaña, J., Cárdenas, V. H., & Motta, V. 2014, *JCAP*, 1410, 017  
 Magaña, J., Motta, V., Cárdenas, V. H., & Foëx, G. 2017, *MNRAS*, 469, 47  
 Magaña, J., Motta, V., Cardenas, V. H., Verdugo, T., & Jullo, E. 2015, *Astrophys. J.*, 813, 69  
 McCully, C., Keeton, C. R., Wong, K. C., & Zabludoff, A. I. 2014, *MNRAS*, 443, 3631  
 —. 2017, *ApJ*, 836, 141

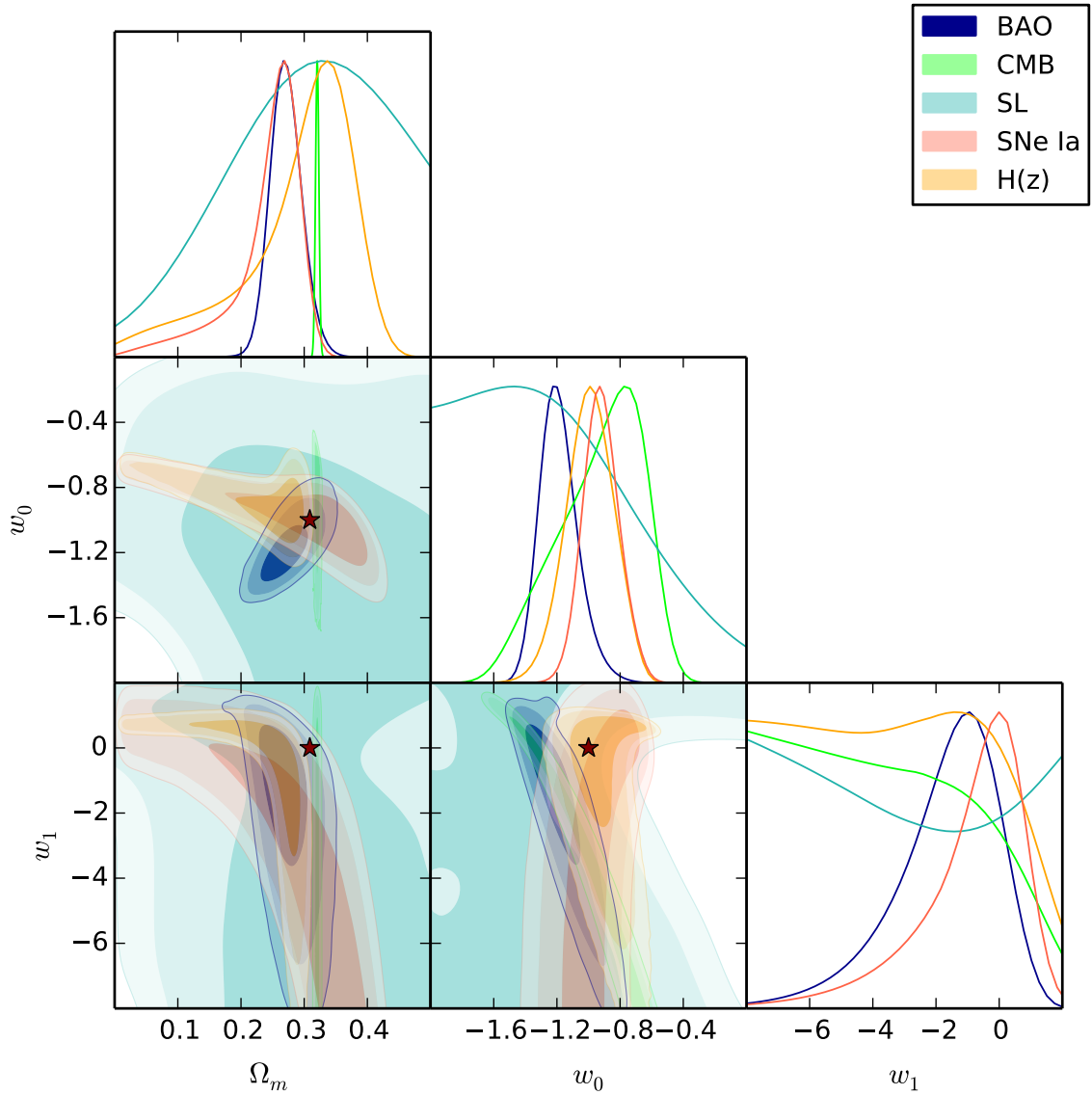


**Figure B3.** The same as Fig. 4 for the FSLL II parameterization.

Meneghetti, M., Natarajan, P., Coe, D., et al. 2016, ArXiv e-prints, arXiv:1606.04548  
 Miralda-Escude, J., & Babul, A. 1995, ApJ, 449, 18  
 Monna, A., Seitz, S., Balestra, I., et al. 2017, MNRAS, arXiv:1605.08784  
 Mortonson, M. J., Weinberg, D. H., & White, M. 2014, ArXiv e-prints, arXiv:1401.0046  
 Neveu, J., Ruhlmann-Kleider, V., Astier, P., et al. 2017, A&A, 600, A40  
 Pantazis, G., Nesseris, S., & Perivolaropoulos, L. 2016, PhRvD, 93, 103503  
 Perlmutter, S., Aldering, G., Goldhaber, G., et al. 1999, The Astrophysical Journal, 517, 565  
 Planck Collaboration, Ade, P. A. R., Aghanim, N., et al. 2016a, A&A, 594, A13  
 —. 2016b, A&A, 594, A14  
 Riess, A. G., Filippenko, A. V., Challis, P., et al. 1998, The Astronomical Journal, 116, 1009  
 Salvatelli, V., Said, N., Bruni, M., Melchiorri, A., & Wands, D. 2014, Phys. Rev. Lett., 113, 181301

Sendra, I., & Lazkoz, R. 2012, MNRAS, 422, 776  
 Soucail, G., Kneib, J.-P., & Golse, G. 2004, A&A, 417, L33  
 Tu, H., Limousin, M., Fort, B., et al. 2008, MNRAS, 386, 1169  
 Umetsu, K., Sereno, M., Medezinski, E., et al. 2015, ApJ, 806, 207  
 Wang, L., Li, C., Kauffmann, G., & De Lucia, G. 2006, MNRAS, 371, 537  
 Wang, S., Hu, Y., Li, M., & Li, N. 2016, ApJ, 821, 60  
 Wang, Y., Chuang, C.-H., & Mukherjee, P. 2012, PhRvD, 85, 023517  
 Weinberg, S. 1989, Reviews of Modern Physics, 61  
 Zeldovich, Y. B. 1968, Soviet Physics Uspekhi, 11  
 Zhao, G.-B., Raveri, M., Pogossian, L., et al. 2017, Nature Astronomy, 1, 627  
 Zitrin, A., Fabris, A., Merten, J., et al. 2015, ApJ, 801, 44

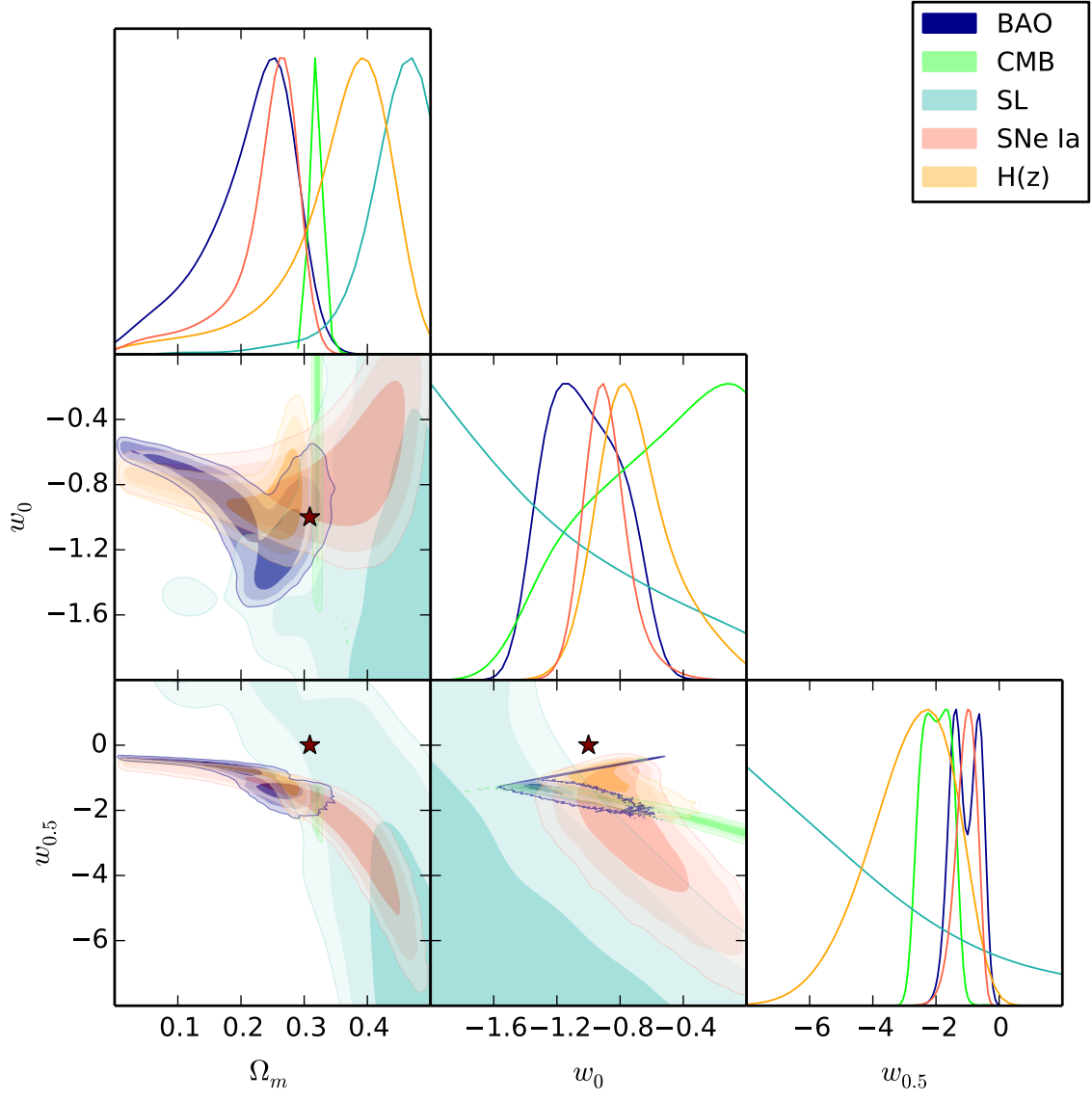


**Figure B4.** The same as Fig. 4 for the SeLa parameterization.